DOI: 10.1002/ejic.201100008

Invariant Oxidation State of Copper but not of Ruthenium in Complexes with Noninnocent *N*-(2-Methyl-5,8-dioxo-5,8-dihydroquinolin-7-yl)acetamide: A Combined Structural, Electrochemical and Spectroelectrochemical Investigation

Alexa Paretzki,[a] Hari Sankar Das,[a] Fritz Weisser,[a] Thomas Scherer,[a] Denis Bubrin,[a] Jan Fiedler,[b] Jacek E. Nycz,[c] and Biprajit Sarkar*[a]

Keywords: Copper / Ruthenium / Quinones / EPR spectroscopy / Electrochemistry / Spectroelectrochemistry / Noninnocent ligands

The compounds [(dppf)Cu(**L**)](BF_4) (**1**[BF_4]) [dppf = 1,1′-bis(diphenylphosphanylferrocene), **L** = *N*-(2-methyl-5,8-dioxo-5,8-dihydroquinolin-7-yl)acetamide] and [$(acac)_2$Ru(**L**)] (**2**) (acac = acetylacetonato) were prepared from the reactions of [Cu(dppf)$(CH_3CN)_2$](BF_4) or [Ru$(acac)_2(CH_3CN)_2$], respectively with **L**. Structural characterization of **1**[BF_4] shows a distorted tetrahedral coordinated copper center. Both complexes show one-electron reversible oxidation as well as reduction processes in their cyclic voltammogram. The first oxidation process of **1**[BF_4] leads to absorptions at around 900 nm in the UV/Vis/NIR spectrum and results in an EPR silent species up to 110 K thus indicating a dppf-centered oxidation. The reduction processes of **1**[BF_4] show features in the UV/Vis/NIR, IR as well as EPR spectrum that are compatible with **L**-centered redox processes. In contrast to this, the ruthenium complex **2** shows metal-centered spin in both the one-electron oxidized as well as reduced forms. These results show that the copper center does not participate in the redox processes in **1**[BF_4] whereas the ruthenium center participates strongly in the electron-transfer processes in **2**. Results obtained from electrochemistry as well as from UV/Vis/NIR, IR, and EPR spectroelectrochemistry are invoked to show the noninnocent nature of **L** in these complexes as well as the more relative importance of metal–**L** covalency in **2** as compared to **1**[BF_4].

Introduction

The copper–quinone interaction plays a vital role in biology[1–5] and chemists have made use of this interaction to build up some fascinating classes of molecules which show many interesting properties.[6–8] Coordination chemists have been attracted towards quinone molecules as ligands for a variety of reasons, the most important to date being the ambiguous valency of their metal complexes.[6,9] After early studies on dithiolenes[10] and dioxolenes,[9] this field has seen a recent surge owing to the availability of advanced spectroscopic techniques and improvement in theoretical methods as well as interest in reactivity studies.[11–17] Such studies have also been performed on metal complexes of other ligands which show valence ambiguity.[18] Ruthenium complexes with quinone ligands present complicated challenges with regard to their valence and spin situation.[19,20] Recent studies have focused on mono as well as multinuclear complexes with quinones[21–26] and other noninnocent ligands.[27–29] Substituted quinoline-5,8-diones have found extensive use in organic and medicinal chemistry owing to their potent antitumor activity.[30–32] Such compounds which combine a *p*-quinone part condensed with a pyridine part have several binding sites available for one or more metal centers. The compound *N*-(2-methyl-5,8-dioxo-5,8-dihydroquinolin-7-yl)acetamide, **L** can bind to a metal center either through an oxygen atom of the *p*-quinone ring and the pyridine nitrogen atom or through the N–H group (before or after deprotonation) together with the oxygen atom. Each of these cases would result in the formation of five-membered chelate rings. Additionally, other less likely coordinations resulting in a four-membered chelate ring or a monodentate coordination are also possible. The ligand **L** combines the "guilty" and noninnocent *p*-quinone as well as the "suspect" pyridine. The *p*-quinone part is a potentially reversible electron transfer site and the presence of several carbonyl groups in **L** provides for good IR spectroscopic handles to verify bonding as well as the redox level of **L**. This is not usually the case for most of the quinone ligands used in the literature because the C–O stretching frequencies in those cases (particularly for the reduced forms of the ligands) fall in the fingerprint region and hence

[a] Institut für Anorganische Chemie, Universität Stuttgart, Pfaffenwaldring 55, 70550 Stuttgart, Germany
Fax: +49-711-68564165
E-mail: sarkar@iac.uni-stuttgart.de
[b] J. Heyrovský Institute of Physical Chemistry, v.v.i., Academy of Sciences of the Czech Republic, Dolejškova 3, 18223 Prague, Czech Republic
[c] Department of Organic Chemistry, Institute of Chemistry, University of Silesia, ul. Szkolna 9, 40-006 Katowice, Poland
Supporting information for this article is available on the WWW under http://dx.doi.org/10.1002/ejic.201100008.

identifying them becomes difficult. In view of the coordination ambiguity, potentially noninnocent character, presence of convenient spectroscopic handles in **L** as well as our general interest in building up metal complexes with new quinone-based ligands,[25,26,33,34] we ventured out to probe its reactions with [Cu(dppf)$(CH_3CN)_2$](BF_4), dppf = 1,1′-bis(diphenylphosphanylferrocene) as well as with [Ru$(acac)_2$-$(CH_3CN)_2$] (acac = acetylacetonato). Both copper and ruthenium complexes of quinone-based ligands are known to show valence and spin ambiguity with various oxidation levels of the ligand and metal center that might occur depending on intramolecular electron transfer. Herein we report on the synthesis of [(dppf)Cu(**L**)](BF_4) (**1**[BF_4]) and [(acac)Ru(**L**)] (**2**). Cu^I as well as Ru^{II} centers are usually prone to undergo intramolecular electron transfer when combined with the completely oxidized form of a quinone ligand. Information on such processes can be vital when trying to determine reactivity of such complexes. By using the ligand **L** we show here how the extent of this electron transfer differs depending on the use of either Cu^I or Ru^{II} centers. The Cu^I precursor was chosen because of the known importance of the copper–quinone interaction and the utility of dppf in providing additional stabilization as well as an additional redox-active site ("ferrocene" center).[35,36] The "[Ru$(acac)_2$]" component was chosen because of the relatively electron-rich nature (vide infra) of the Ru^{II} center in that part. Structural data are used to discuss the bonding situation in the copper complex. A combination of electrochemical as well as UV/Vis/NIR, IR, and EPR (Electron Paramagnetic Resonance) spectroelectrochemical results are used to answer questions related to electron transfer and valence and spin distribution.

Results and Discussion

Synthesis and Crystal Structure

Compounds **1**[BF_4] and **2** (Scheme 1) were synthesized by the reactions of **L** with [Cu(dppf)$(CH_3CN)_2$]BF_4 or [Ru$(acac)_2(CH_3CN)_2$], respectively, in CH_2Cl_2 or EtOH. Attempts to prepare the corresponding complex with the $Ru(bpy)_2Cl_2$ (bpy = 2,2′-bipyridine) precursor, even after removal of the chloride ions by Ag^I salts, were not successful and showed the competition for metal dπ electrons between bpy and **L** which does not allow sufficient Ru–**L** π-bonding interaction that would stabilize coordination of the rather poor σ-donating ligand **L**. Whereas **1**[BF_4] could be purified by recrystallization, **2** had to be purified by column chromatography on an alumina column (see Exp. Section). The purity of the complexes was verified with ^1H- and ^{31}P NMR spectroscopy, elemental analysis, and mass spectrometry.

1[BF_4] could be crystallized from a mixture of dichloromethane and *n*-hexane (1:5) as a dichloromethane solvate. The compound crystallized in the triclinic $P\bar{1}$ space group. Crystallographic details are presented in Table 5 and selected bond lengths and bond angles are given in Table 1.

Table 1. Selected bond lengths [Å] and bond angles [°].

Selected bond lengths	
Cu–N1	2.024(6)
Cu–P2	2.239(2)
Cu–P1	2.258(3)
Cu–O1	2.271(5)
O1–C8	1.243(8)
N1–C1	1.353(8)
N1–C9	1.393(8)
C1–C2	1.410(9)
C1–C111	1.504(9)
O2–C5	1.238(8)
N2–C71	1.397(9)
N2–C7	1.386(8)
C2–C3	1.42(1)
C3–C4	1.363(9)
O3–C71	1.226(8)
C4–C9	1.398(9)
C4–C5	1.49(1)
C5–C6	1.45(1)
C6–C7	1.334(9)
C7–C8	1.513(9)
C8–C9	1.461(9)
C71–C72	1.49(1)
Selected bond angles	
N1–Cu–P2	126.5(2)
N1–Cu–P1	116.5(2)
P2–Cu–P1	114.68(9)
N1–Cu–O1	77.7(2)
P2–Cu–O1	110.8(1)
P1–Cu–O1	97.0(1)

The Cu^I center in **1**[BF_4] is in a distorted tetrahedral environment being coordinated by an oxygen and a nitrogen atom of **L** and by the phosphorus atoms of dppf (Figure 1). The distortion is imposed by the chelating nature of the dppf and L ligands. Thus the N1–Cu–O1 angle is 77.7(2)°, and the P1–Cu–P2 angle is 114.68°. The Cu–O1 and Cu–P1 distances at 2.271(5) and 2.258(3) Å are longer than the Cu–N1 and Cu–P2 distances of 2.024(6) and 2.239(2) Å,

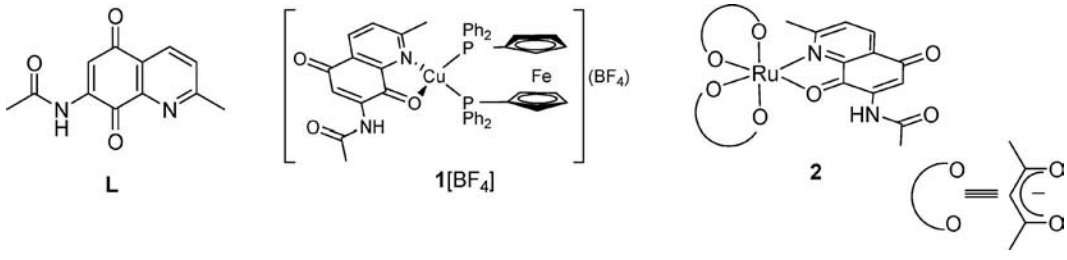

Scheme 1.

respectively, and accordingly, the O1–Cu–P1 angle of 97.0(1)° is smaller than the N1–Cu–P2 angle of 126.5(2)°. The Cu–O1 bond length at 2.271(5) Å is relatively long and this is in keeping with an unreduced C=O group in the ligand **L** (vide infra). A close look at the bond lengths within the ligand **L** shows that the C8–O1 distance of 1.243(8) Å is only slightly longer than the C5–O2 and C71–O3 distances of 1.238(8) and 1.226(8) Å, respectively. This is a first indication of the unreduced state of the ligand **L** in this complex. The slight elongation of the C8–O1 distance as compared to an authentic C=O carbonyl double bond has to do with slight back-donation from the Cu^{I} center to the π* orbital of **L**. The C4–C9 and C6–C7 distances of 1.398(9) and 1.334(9) Å, respectively, are shorter than the other distances in this ring containing the carbonyl groups and hence it is seen that the ligand retains its unreduced quinone form after coordination to the Cu^{I} center. For comparison, the free ligand **L** has C4–C9 and C6–C7 distances of 1.388(2) and 1.352(2) Å, respectively which are very close to the distances observed in its Cu^{I} coordinated form. The distance between the N–H (N2) part of the amide group and the coordinated oxygen (O1) atom is 2.29 Å. The "ferrocene" part of dppf adopts a staggered conformation with a pseudo local D_{5d} symmetry. The distance between the copper and the iron centers is 4.025 Å. Despite several attempts at crystallizing **2**, we were not able to obtain suitable crystals for carrying out single-crystal X-ray diffraction measurements.

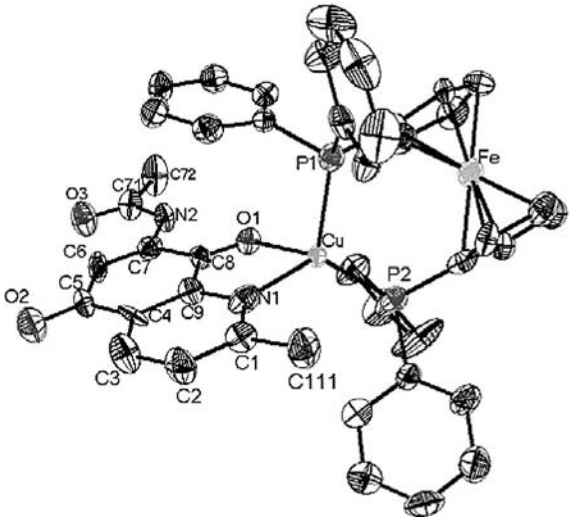

Figure 1. ORTEP plot of **1**[BF_4]·CH_2Cl_2. Ellipsoids drawn at 30% probability. The counteranion, CH_2Cl_2 and protons are not shown for the sake of clarity.

Cyclic Voltammetry

Cyclic voltammetry experiments were carried out on the complexes in order to investigate their redox properties. Both complexes show one one-electron oxidation and two one-electron reductions in CH_2Cl_2/0.1 M Bu_4NPF_6 at 295 K (Figure 2 and Figure S1). Whereas the first oxidation as well as reduction processes were completely reversible for **2**, complex $\mathbf{1}^+$ showed only a fully reversible first reduction; the other redox processes for $\mathbf{1}^+$ were either quasireversible or irreversible. The free ligand **L** shows two one-electron reduction processes at –0.98 and –1.47 V in CH_2Cl_2/0.1 M Bu_4NPF_6 at 295 K vs. Fc^0/Fc^+ (Figure S1). Compared to the reduction potentials of **L**, the potentials of $\mathbf{1}^+$ are anodically shifted (Table 2). This is probably due to the σ-polarization of **L** induced by coordination of the Cu^{I} center as well as the relatively small π back-bonding from the Cu^{I} center to **L** as established from crystal structure analysis. Such metal-coordination-induced shifts of reduction potentials are well established for π-acceptor-type ligands of which **L** is an example. Interestingly, the second reduction of the complex $\mathbf{1}^+$ is much less shifted in comparison to the free ligand. However, this is not surprising in the current case of the dioxolene redox series (quinone-semiquinone-diphenolate) when only one of the oxygen atoms is coordinated to the metal center. The first reduction of $\mathbf{1}^+$ is reversible only at higher scan rates and lower temperatures (233 K). Reduction at slower scan rates leads to ligand dissociation as has been proved by comparison with the cyclic voltammogram of **L** (Figure S1, bottom). The second reduction of $\mathbf{1}^+$ is irreversible at all tested scan rates and temperatures. Complex **2** shows a reversible one-electron oxidation process at low positive potentials and two one-electron reduction processes, the potentials of which are only slightly shifted compared to **L**. In order to gain more insight into the redox processes of $\mathbf{1}^+$ and **2** as well as to make a possible assignment of them we carried out a combination of UV/Vis/NIR, IR, and EPR spectroelectrochemical measurements.

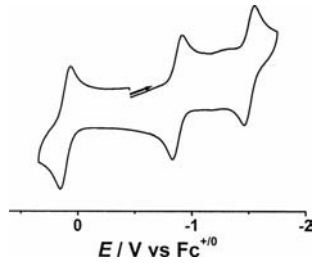

Figure 2. Cyclic voltammogram of **2** in CH_2Cl_2/0.1 M Bu_4NPF_6 at 295 K. The Fc^0/Fc^+ couple was used as an internal standard.

Table 2. Electrochemical data.[a]

Compound	$E_{1/2}$(ox)	$E_{1/2}$(red1)	$E_{1/2}$(red2)
L	–	–0.98	–1.47
$\mathbf{1}^+$	0.43	–0.57	–1.42[b]
2	0.11	–0.87	–1.51

[a] Electrochemical potentials from cyclic voltammetry in CH_2Cl_2/0.1 M Bu_4NPF_6 at 295 K. The Fc^0/Fc^+ couple was used as an internal standard. [b] Cathodic peak potential for irreversible reduction.

IR Spectroelectrochemistry

The assignment of IR bands of **L** (Figure S2) is complicated because of coupling of C=O stretchings with ring vi-

brations and possible shifts due to Fermi resonance. Furthermore, a hydrogen bond from the N–H group to neighboring carbonyl on the quinone ring can weaken this C=O bond and shift the stretching frequency to a lower value. Tentatively we ascribe the bands 1685 and 1652 cm^{-1} to quinone (C5, C8) C=O stretchings in analogy to the assignment for the benzoquinone molecule [υ(CO) = 1686 and 1666 cm^{-1}]. The band at higher wavenumbers 1719 cm^{-1} remains almost unchanged after coordination of **L** to metals (Table 4) and can be assigned to the C=O stretching of the amide group. The N–H stretching vibration of the amide group appears at 3367 cm^{-1}. On one-electron reduction to $\mathbf{L}^{\cdot-}$ the bands in the carbonyl and ring vibration region are shifted to lower frequencies (Figure S2, Table 3) and the overall character of the spectrum (shape, separation of bands) seems to be largely changed. The shift of the bands to lower frequencies can be explained by the population of an antibonding orbital on one-electron reduction; the dislocation of bands is probably influenced by the formation of a stronger O···H hydrogen bond between the C=O (C8) group and the amide N–H group in the more electron-rich one-electron reduced species. The hydrogen bond also weakens the N–H bond which results in the shift of its stretching band to 3319 cm^{-1}.

Table 3. IR data of ligand and complexes.[a]

Compound	ν [cm^{-1}]
$\mathbf{L}^{\cdot-}$	3319, 1682, 1585, 1533
L	3367, 1719, 1685, 1652, 1620, 1591
$\mathbf{1}^{\cdot}$	3360, 1688, 1579, 1540
$\mathbf{1}^{+}$	3392, 1720, 1657, 1610, 1590, 1567
$\mathbf{1}^{2+}$	3390, 1719, 1656, 1610, 1590, 1567
$\mathbf{2}^{\cdot-}$	3380, 1680, 1567, 1547
2	3386, 1708, 1601, 1547
$\mathbf{2}^{\cdot+}$	3385, 1726, 1654, 1590

[a] From measurements in CH_2Cl_2/0.1 M Bu_4NPF_6 (OTTLE spectroelectrochemistry).

Complex $\mathbf{1}^{+}$ exhibits two bands in the range of the original free ligand carbonyl stretchings which can be ascribed to the amide C=O (band at 1720 cm^{-1}) and to the free (uncoordinated) C=O on the quinone ring (C5) (band at 1657 cm^{-1}). The third, coordinated carbonyl (C=O of C8) is expectably more shifted and occurs around 1600 cm^{-1}, merged in the ring vibration bands. The N–H stretching vibration appears at 3392 cm^{-1} (Figure 3). Comparison of the band frequencies with those of the free ligand (Table 3) shows some interesting consequences that result out of bonding of the copper center. The N–H band shifts to higher wavenumbers on coordination of the Cu^{I} center, the amide C=O stays invariable, the C=O (C5) shows a low energy shift of 28 cm^{-1} and the C=O (C8) shows a low energy shift of more than 40 cm^{-1}. The high energy shift of the N–H bond on Cu^{I} coordination shows the marginal back-donation in this system. The N–H group competes with the Cu^{I} center for the oxygen lone pairs and hence the hydrogen bonding to C=O (C8) becomes weaker and the N–H bond stronger. Coordination of Cu^{I} results in weakening of the C=O bond because of lone pair donation and hence a low energy shift. The one-electron oxidized product was detected by scanning the potential in the spectroelectrochemical experiment back before the onset of the decomposition product (see Exp. Section). One-electron oxidation to $\mathbf{1}^{2+}$ results in a spectrum that is almost identical to $\mathbf{1}^{+}$ (Figure S3). This is a first indication that the oxidation takes place in the dppf part of the molecule. On one-electron reduction to $\mathbf{1}^{\cdot}$, all the aforementioned bands including the N–H band shift to lower energies. The amide C=O band appears at 1688 cm^{-1}, both quinone C=O bands are positioned at quite low wavenumbers, in the region of ring vibrations (Figure 3). The resulting spectrum rather resembles the spectrum of $\mathbf{L}^{\cdot-}$ (Figure S2, Table 4) thus indicating an **L**-centered reduction in **1**. The low energy shift of the N–H band on moving from $\mathbf{1}^{+}$ to $\mathbf{1}^{\cdot}$ can be explained by the enhanced hydrogen bonding between N–H and C=O (C8) in the comparatively electron-rich $\mathbf{L}^{\cdot}$ in $\mathbf{1}^{\cdot}$.

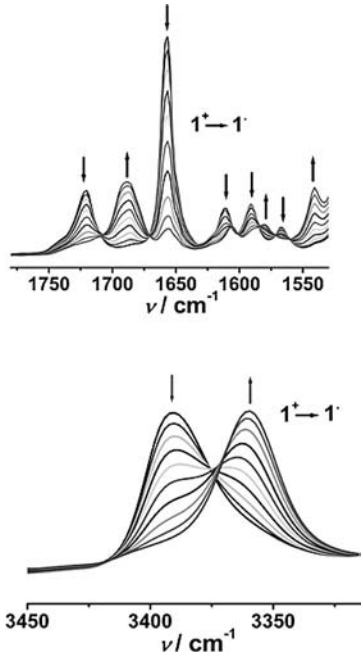

Figure 3. Changes in the IR spectrum of $\mathbf{1}^{+}$ during first reduction in CH_2Cl_2/0.1 M Bu_4NPF_6. Top: carbonyl region, bottom: N–H region.

In contrast to $\mathbf{1}^{+}$, the ruthenium complex **2** shows all C=O stretching bands at lower frequencies in comparison to free ligand. Particularly the quinone C=O frequencies at 1601 and 1547 cm^{-1} are closer to frequencies of $\mathbf{L}^{\cdot-}$ than to those of unreduced **L**, the amide C=O lies at 1708 cm^{-1} (Figure 4, Table 3). These values are indicative of a large back-donation from the Ru^{II} center to **L** in **2** and the importance of covalency in such ruthenium complexes. Complex **2** would thus be described as a resonance hybrid of Ru^{II}–**L** and Ru^{III}–$\mathbf{L}^{\cdot-}$. Influence of the electronic spin of Ru^{III} and the radical form $L^{\cdot-}$ (paramagnetic shift) on the ^1H NMR spectrum of **2** is not observed. This is because of the antiferromagnetic coupling of the two spins which results in a diamagnetic complex. Similar situations are known in the literature for singlet diradicals. This result dif-

Table 4. UV/Vis/NIR data of ligands and complexes.[a]

	λ_{max} [nm] (ε [$M^{-1}cm^{-1}$])
$\mathbf{L}^{\cdot-}$	242 (6700), 268 (8400), 300 (8900), 404 (9400), 477 (8500), 630 (1700)
L	242 (6400), 265 (7500), 299 (8000), 377 (1500)
$\mathbf{1}^{\cdot}$	243 (16900), 266 (18600), 303 (19400), 399 (8800), 458 (8900), 532 (600)
$\mathbf{1}^{+}$	240 (14800), 269 (16600), 300 (16800), 590 (2600)
$\mathbf{1}^{2+}$	243 (14700), 267 (16400), 300 (17200), 414 (4300), 497 sh, 600 sh
$\mathbf{2}^{\cdot-}$	243 (14800), 270 (18100), 296 (17600), 392 (8100), 500 (5600), 570 (4000), 1217 (6500)
2	240 (13500) 270 (18200), 353 (7100), 463 (7000), 743 (6700)
$\mathbf{2}^{+\cdot}$	239 (13600), 270 (16700), 297 (15100), 327 (11000), 630 (5700)

[a] Measurements in CH_2Cl_2/0.1 M Bu_4NPF_6 (OTTLE spectroelectrochemistry).

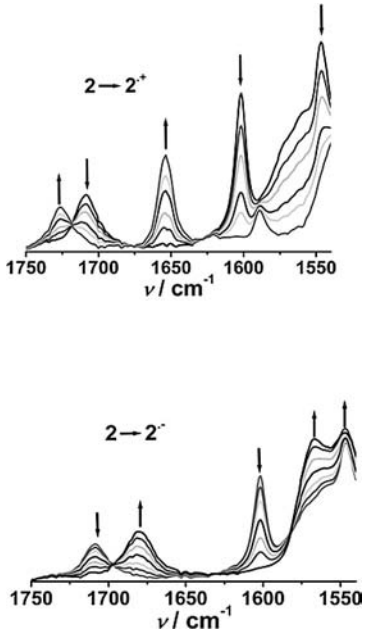

Figure 4. Changes in the IR spectrum of **2** during first oxidation (top) and first reduction (bottom) in CH_2Cl_2/0.1 M Bu_4NPF_6.

fers strongly from that of $\mathbf{1}^{+}$ where IR results indicate an unreduced **L** and almost nonexistent back-donation from the Cu^{I} center to **L**. One-electron oxidation to $\mathbf{2}^{\cdot+}$ shifts all the C=O bands to higher wavenumbers (Figure 4 and Table 3) and these values are now closer to those of **L**. The still lower stretching frequencies (1654 and 1590 cm^{-1}) of the two C=O (C5 and C8) groups in comparison to the values for the free ligand (1685 and 1652 cm^{-1}) can be explained by back-donation from the ruthenium center. The ruthenium center in this case is comparatively "electron rich" even in higher oxidation states because of the presence of donating ligands such as acac. One-electron reduction to $\mathbf{2}^{\cdot-}$ shifts all the C=O bands to lower energies and these values are now compatible with $\mathbf{L}^{\cdot-}$ and $\mathbf{1}^{\cdot}$ thus showing the presence of $\mathbf{L}^{\cdot-}$ in $\mathbf{2}^{\cdot-}$ (Table 3 and Figure 4). The N–H stretching bands in **2**, $\mathbf{2}^{\cdot-}$, and $\mathbf{2}^{\cdot+}$ appear at almost identical frequencies showing the negligible effects of the redox processes of **2** on the strength of the N–H bond in these complexes and probably weaker influence of the hydrogen bond N–H···O=N. The lack of complete reversibility of the second reduction process in the longer time scale of the OTTLE measurement precluded the identification of IR bands for both $\mathbf{2}^{2-}$ and $\mathbf{1}^{-}$.

UV/Vis/NIR Spectroelectrochemistry

The free ligand **L** shows absorptions in the UV region and one in the visible region at 377 nm which can be assigned to a $\pi \rightarrow \pi^*$ transition (Table 4 and Figure S4). On reduction to $\mathbf{L}^{\cdot-}$ in CH_2Cl_2/0.1 M Bu_4NPF_6, new bands show up in the visible region at 477 nm (8500 $M^{-1}cm^{-1}$) and 630 nm (1700 $M^{-1}cm^{-1}$, Figure S4). Such low energy bands are typical for organic radicals because of the low energy gap between the singly occupied molecular orbital (SOMO) generated on one-electron reduction and other close-lying higher energy empty orbitals. The bands in the UV region of **L** remain unaltered on one-electron reduction.

Complex $\mathbf{1}^{+}$ shows bands in the UV region that are assigned to **L**-centered transitions (Figure 5 and Table 4). Additionally, a transition is observed at 590 nm (2600 $M^{-1}cm^{-1}$) which can be assigned to a d(Cu,Fe) → π^*(**L**) MLCT transition. On one-electron oxidation to $\mathbf{1}^{2+}$, the MLCT band shifts to 414 nm. Unambiguous identifica-

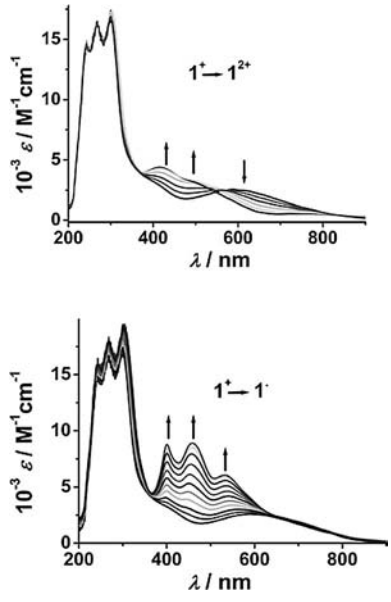

Figure 5. Changes in the UV/Vis/NIR spectrum of $\mathbf{1}^{+}$ during first oxidation (top) and first reduction (bottom) in CH_2Cl_2/0.1 M Bu_4NPF_6.

tion of the expected band at around 600 nm for oxidation of dppf is difficult in the present case because of overlap with the MLCT band.[37] On reduction to $\mathbf{1}^{\cdot}$, new bands appear at 532 nm (600 $M^{-1}cm^{-1}$), 458 nm (8900 $M^{-1}cm^{-1}$), and 399 nm (8800 $M^{-1}cm^{-1}$) (Table 4 and Figure 5). These bands are reminiscent of the bands observed in $\mathbf{L}^{\cdot-}$ and are assigned to intraligand transitions thus corroborating the IR spectroelectrochemical results of a **L**-centered reduction in $\mathbf{1}^{\cdot}$. The MLCT band in this case is overlapped by the intraligand transitions seen in the visible region. The bands in the UV region of $\mathbf{1}^{+}$ remain unaltered on one-electron oxidation as well as one-electron reduction.

Complex **2** shows the expected d(Ru)→π*(L) MLCT band in the visible region at 743 nm (ε = 6700 $M^{-1}cm^{-1}$) and an additional band at shorter wavelengths (463 nm, ε = 7000 $M^{-1}cm^{-1}$) which we attribute to MLCT from Ru to energetically higher (in comparison to L) π* orbitals of acac. One-electron oxidation to $\mathbf{2}^{\cdot+}$ results in a hypsochromic shift of the MLCT bands (Figure 6 and Table 4). On reduction to $\mathbf{2}^{\cdot-}$, a new relatively intense band emerges in the NIR region at 1217 nm (6500 $M^{-1}cm^{-1}$) which can be assigned to a ligand-to-metal charge transfer (LMCT) transition from $\mathbf{L}^{\cdot-}$ (SOMO) to d(Ru) (Figure 6 and Table 4).[21] Such low-energy LMCT bands with radical ligands have precedence in the literature. Additionally, $\mathbf{2}^{\cdot-}$ shows bands at 570, 500, and 392 nm that are reminiscent of the bands observed in the case of $\mathbf{L}^{\cdot-}$ and are hence assigned to intraligand (IL) transitions based on $\mathbf{L}^{\cdot-}$. The absorptions in the UV region remain unchanged in the case of all redox forms of **2**. The instability of the two-electron reduced forms of the complexes in the timescale of spectroelectrochemical experiments precluded the identification of bands for both $\mathbf{2}^{2-}$ and $\mathbf{1}^{-}$.

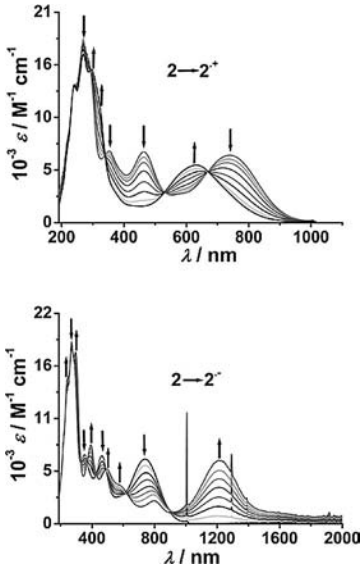

Figure 6. Changes in the UV/Vis/NIR spectrum of **2** during first oxidation (top) and first reduction (bottom) in CH_2Cl_2/0.1 M Bu_4NPF_6.

EPR Spectroscopy

EPR spectroscopy was used to determine the electron density distribution for the paramagnetic species reported in this work and shows some interesting effects particularly for $\mathbf{2}^{\cdot+}$ and $\mathbf{2}^{\cdot-}$. The one-electron oxidized form $\mathbf{1}^{2+}$ did not show any defined EPR signals between 295 and 110 K in CH_2Cl_2/0.1 M Bu_4NPF_6. This indicates a dppf-based oxidation because of the well-known fast relaxation rates arising out of degenerate orbitals as in the case of ferrocenium. This observation thus supplements the IR and UV/Vis/NIR spectroelectrochemical studies that also point to a dppf-centered oxidation in $\mathbf{1}^{2+}$ which is best described as $[(dppf)^{+}Cu^{I}(\mathbf{L})]^{2+}$. The in situ-generated one-electron reduced form $\mathbf{1}^{\cdot}$ showed a well-resolved signal at 295 K that is centered around g = 2.005. This spectrum could be simulated with the parameters $^{63,65}Cu$ (I = 3/2), 2.9 G; 2 X ^{31}P (I = 1/2), 6 G; ^{14}N (I = 1), 4.8 G and ^{1}H (I = 1/2), 1.6 G (Figure 7). Such values are typical for radicals bound to the Cu(dppf) unit. These data point clearly to a **L**-centered reduction and $\mathbf{1}^{\cdot}$ is thus formulated as $[(dppf)Cu^{I}(\mathbf{L}^{\cdot-})]^{\cdot}$.

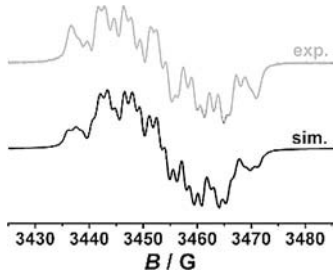

Figure 7. EPR spectrum of in situ electrochemically generated $\mathbf{1}^{\cdot}$ in CH_2Cl_2/0.1 M Bu_4NPF_6 at 233 K (top) with simulation (bottom).

The one-electron oxidized form $\mathbf{2}^{+}$ of the ruthenium complex is EPR silent at 295 K. At 110 K, an axially symmetric signal is observed with $g_{\perp}$ = 2.269 and $g_{\parallel}$ = 1.798. The large g anisotropy ($\Delta g = g_{\perp} - g_{\parallel}$) of 0.471 and the g_{av} value of 2.112 point clearly to ruthenium-centered spin which is compatible with a $[(acac)_2Ru^{III}(\mathbf{L})]^{+}$ description for $\mathbf{2}^{+}$. Suprisingly, the one-electron reduced species $\mathbf{2}^{\cdot-}$ is also EPR silent at 295 K. At 110 K this species shows an axial symmetric signal as well with $g_{\perp}$ = 2.213 and $g_{\parallel}$ = 1.809. The g_{av} is 2.078 and the g anisotropy ($\Delta g = g_{\perp} - g_{\parallel}$) is 0.404. Although the Δg value in this case is smaller than that for $\mathbf{2}^{\cdot+}$, this value as well as the g_{av} value point to a

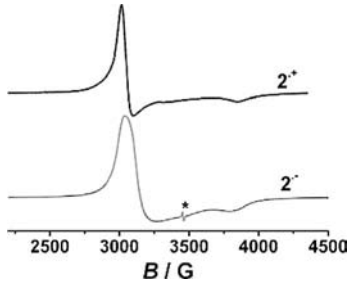

Figure 8. EPR spectrum of in situ electrochemically generated $2^{\cdot+}$ (top) and 2^{-} (bottom) in CH_2Cl_2/0.1 M Bu_4NPF_6 at 110 K. * denotes an organic impurity generated during reduction.

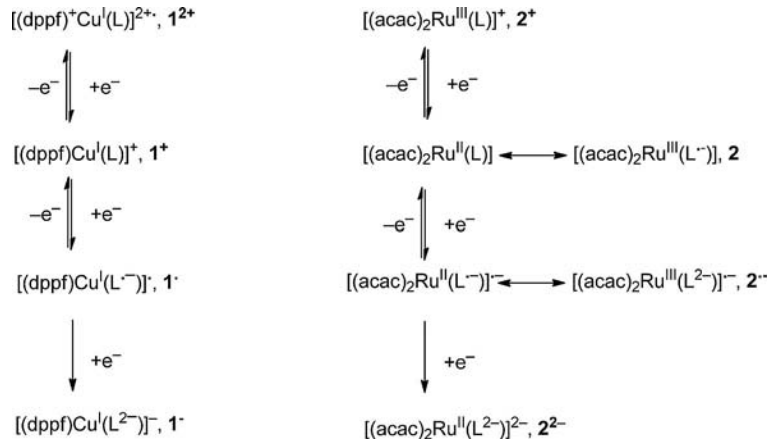

Scheme 2.

substantial amount of ruthenium-centered spin also for $\mathbf{2}^{\cdot-}$ (Figure 8). Taking into consideration the IR and UV/Vis/NIR data, this species would then be best formulated as a resonance hybrid of $[(acac)_2Ru^{II}(\mathbf{L}^{\cdot-})]^{-}$ and $[(acac)_2Ru^{III}(L^{2-})]^{\cdot-}$.

Discussion of Structural and Combined Spectroscopic Results

For complex $\mathbf{1}^{+}$ bond length analysis inside the ligand **L** and comparison of these values with those from free **L** point to an unreduced **L** and unambiguously establish the form $[(dppf)Cu^{I}(\mathbf{L})]^{+}$. This is corroborated by the IR stretching frequencies of the C=O groups in bound **L**, which are very similar to those of free **L**, and the EPR silence of $\mathbf{1}^{+}$. One-electron oxidation to $\mathbf{1}^{2+}$ produces a species that is EPR silent till 110 K and shows an IR signature that is almost identical to $\mathbf{1}^{+}$. These data strongly point to a dppf-centered oxidation since a Cu^{II}-based EPR signal should certainly be visible at least at 110 K. Thus, $\mathbf{1}^{2+}$ is best formulated as $[(dppf)^{+}Cu^{I}(\mathbf{L})]^{2+}$. One-electron reduction to $\mathbf{1}^{\cdot}$ generates a UV/Vis/NIR spectra showing intraligand transitions with vibrational structure in the visible region as also observed for free $\mathbf{L}^{\cdot-}$. The EPR spectrum of $\mathbf{1}^{\cdot}$ at room temperature shows a *g* value close to the free electron value and hyperfine couplings to ^{14}N, ^{31}P, ^{1}H, and $^{63,65}Cu$ nuclei which are completely in line with an organic radical. The C=O stretching frequencies are also compatible with those of free $\mathbf{L}^{\cdot-}$. These data thus conclusively prove the formulation of $\mathbf{1}^{\cdot}$ as $[(dppf)Cu^{I}(\mathbf{L}^{\cdot-})]^{\cdot}$. Further one-electron reduction to $\mathbf{1}^{-}$ in all likelihood produces the species $[(dppf)Cu^{I}(\mathbf{L}^{2-})]^{-}$.

In the absence of structural data, IR spectroscopy together with EPR data helps in the assignment of **2**. The extremely large shifts to lower energy observed for the C=O stretching frequencies of the ligand **L** in **2** compared to its free form indicates a strong amount of back-bonding from the Ru^{II} center to the ligand **L**. Simple coordination-induced shifts are likely to be much smaller than what is observed in the present case. These data together with the EPR silence of this species till 110 K points to a resonance hybrid between the forms $[(acac)_2Ru^{II}(\mathbf{L})]$ and the spin-coupled $[(acac)_2Ru^{III}(\mathbf{L}^{\cdot-})]$. One-electron oxidation to $\mathbf{2}^{+}$ produces a species that is EPR silent at room temperature but shows a signal at 110 K which has a large *g*-anisotropy and g_{av} value very different from that of the free electron value. This is a clear indication of metal-centered spin and is compatible with literature reports of Ru^{III}-based EPR signals. Thus, strong support from EPR data together with the IR spectroscopic results point to the formulation of $\mathbf{2}^{+}$ as $[(acac)_2Ru^{III}(\mathbf{L})]^{+}$. One-electron reduction to $\mathbf{2}^{\cdot-}$ produces a species where the IR and UV/Vis/NIR signatures are reminiscent of free $\mathbf{L}^{\cdot-}$. This is seen in the large low energy shifts of the C=O stretching frequencies as well as the appearance of intraligand bands with vibrational structure in the visible region. These data would point to the formulation of $\mathbf{2}^{\cdot-}$ as $[(acac)_2Ru^{II}(\mathbf{L}^{\cdot-})]^{\cdot-}$. However, the EPR signal for $\mathbf{2}^{\cdot-}$ which is observed only at 110 K is very similar to that observed for $\mathbf{2}^{+}$ and indicates substantial Ru^{III} character for this species. Thus, these combined data point to a best description of $\mathbf{2}^{\cdot-}$ as a resonance hybrid between $[(acac)_2Ru^{II}(\mathbf{L}^{\cdot-})]^{-}$ and $[(acac)_2Ru^{III}(\mathbf{L}^{2-})]^{\cdot-}$. Further one-electron reduction to $\mathbf{2}^{2-}$ in all likelihood produces $[(acac)_2Ru^{II}(\mathbf{L}^{2-})]^{2-}$ (Scheme 2).

Conclusions

By using the noninnocent ligand *N*-(2-methyl-5,8-dioxo-5,8-dihydroquinolin-7-yl)acetamide we could show that relatively electron-rich metal centers are required to form stable complexes with it. **L** binds to metal centers through the pyridine nitrogen atom and the O atom connected to C8. Crystallographic as well as IR spectroscopic investigation of the copper complex $\mathbf{1}^{+}$ showed a negligible amount of Cu^{I} to **L** back-bonding in this case thus stabilizing this quinone-containing ligand in its unreduced form in $\mathbf{1}^{+}$. A combination of IR, UV/Vis, and EPR spectroelectrochemical results on $\mathbf{1}^{+}$ and its various redox forms point clearly to dppf-centered oxidation in $\mathbf{1}^{2+}$ and **L**-centered reduction in $\mathbf{1}^{\cdot}$ thus leaving the Cu^{I} oxidation state unaltered in all the redox forms of $\mathbf{1}^{+}$. In contrast, the ruthenium complex **2** shows a more complex situation where the ruthenium center participates in the redox processes, the amount of back-

donation is large and the redox states show a mixed type of valence situation pointing to the importance of covalency in metal complexes of ruthenium. The observed results for the copper and ruthenium complexes are summarized in Scheme 2.

Experimental Section

General Considerations: The complexes *cis*-$Ru(acac)_2(CH_3CN)_2$,[38] $[(dppf)Cu(CH_3CN)_2](BF_4)$[39] and the ligand (**L**)[40] were synthesized according to reported procedures. $RuCl_3{\cdot}nH_2O$ was purchased from Merck, CuCl from Strem, and 1,1′-bis(diphenylphosphanyl)ferrocene from Alfa Aesar. All the reagents were used as supplied. For the copper complex, all manipulations were carried out using Schlenk techniques under argon. The solvents used for metal complex syntheses were dried and distilled under argon and degassed by common techniques prior to use.

Instrumentation: The ^1H and $^{31}P\{^1H\}$ NMR spectra were recorded with a Bruker AC 250 spectrometer. Electronic absorption spectra were recorded with J&M TIDAS and Shimadzu UV 3101 PC spectrophotometers. EPR spectra in the X-band were recorded with a Bruker System EMX. IR spectra were obtained using a Nicolet 6700 FTIR instrument. Cyclic voltammetry was carried out in 0.1-M Bu_4NPF_6 solutions using a three-electrode configuration (glassy-carbon working electrode, Pt counter electrode, Ag wire as psuedo-reference) and a PAR 273 potentiostat and function generator. The ferrocene/ferrocenium (Fc^0/Fc^+) couple served as internal reference. Spectroelectrochemistry was performed using an optically transparent thin-layer electrode (OTTLE) cell. Elemental analyses were performed with the Perkin–Elmer Analyzer 240.

Synthesis of [Cu(dppf)L](BF$_4$) (1[BF$_4$]): The ligand **L** (23 mg, 0.1 mmol) and $[Cu(dppf)(CH_3CN)_2]BF_4$ (79 mg, 0.1 mmol) were dissolved in degassed dichloromethane (10 mL) under argon. The solution immediately turned dark blue. After stirring the solution for 18 h at room temperature, the solvent was removed under reduced pressure. The dark-blue solid was recrystallized from dichloromethane/hexane (1:5). ^1H NMR (250 MHz, $CDCl_3$, 298 K): δ = 2.33 (s, 3 H, CH_3-CO-), 2.63 (s, 3 H, CH_3-pyridin), 4.29–4.71 (m, 8 H, Cp-H), 7.28–7.78 (m, 20 H, phenyl-H), 7.85 (d, ^3J = 8.1 Hz, 1 H, pyridine-H), 7.96 (s, 1 H, quinone-H), 8.19 (br. s, 1 H, NH), 8.51 (d, ^3J = 8.1 Hz, 1 H, pyridine-H) ppm. $^{31}P\{^1H\}$ NMR (101.26 MHz, $CDCl_3$, 298 K): δ = –8.15 (s, br) ppm. $C_{46}H_{38}BCuF_4FeN_2O_3P_2{\cdot}0.5CH_2Cl_2$: calcd. C 57.08, H 4.12, N 2.86; found C 57.34, H 4.06, N 2.78.

Synthesis of [Ru(acac)$_2$L] (2): The ligand **L** (0.023 g, 0.10 mmol) and the metal precursor $[Ru(acac)_2(CH_3CN)_2]$ (0.038 g, 0.10 mmol) were dissolved in ethanol (20 mL) and refluxed for 12 h under argon resulting in a color change from orange to dark-green. The solvent of the reaction mixture was evaporated to dryness under reduced pressure and the residue was then purified on an alumina column. The dark-green product was eluted with CH_2Cl_2/CH_3CN (9:1). Evaporation of solvent under reduced pressure afforded the pure complex. Yield: 0.012 g, 23%. ^1H NMR (CD_3CN, 250 MHz, 298 K): δ = 2.06 (s, 3 H, Me), 2.12 (s, 3 H, Me), 2.15 (s, 3 H, Me), 2.26 (s, 3 H, Me), 2.37 (s, 3 H, Me), 2.54 (s, 3 H, Me), 5.31 (s, 1 H, CH_3-C-C*H*), 5.82 (s, 1 H, CH_3-C-C*H*), 7.83 (s, 1 H, C*H*-C-NH), 7.84 (d, $^3J_{HH}$ = 8 Hz, 1 H, C*H*-C-N) 8.4 (d, J_{HH} = 8 Hz, 1 H, C*H*-C-C), 9.65 (br. s, 1 H, NH) ppm. $C_{22}H_{24}N_2O_7Ru$ (529.51): calcd. C 49.90, H 4.57, N 5.29; found C 49.58, H 4.36, N 5.12. MS (ESI): *m*/*z* (%) = 531 ($[M + H]^+$), 553 ($[M + Na]^+$).

X-ray Crystallography: Compound 1[BF_4] was crystallized as a dichloromethane solvate by diffusion of a dichloromethane solution layered with *n*-hexane (1/5). Data collection was made using a four circle diffractometer P4 (Siemens, Madison, USA). The measurements were carried out at 173 K using Mo-K_α radiation (graphite monochromator). Phase problems were solved using the program SHELXTL PC 5.03.[41] Because of the low intensity of the crystal, unique reflections at higher 2-theta angles could not be detected. This circumstance yields a weak data set that is criticized as an A-Alert in the checkCIF report. However, the data set collected is of a reasonable quality and the connectivity as well as bond lengths can be discussed with confidence (Table 5).

Table 5. X-ray crystal structure data for compound 1[BF_4]·CH_2Cl_2.

Chemical formula	$C_{46}H_{38}BCuF_4FeN_2O_3P_2{\cdot}CH_2Cl_2$
M_r	1019.85
Temperature [K]	173(2)
λ [Å]	0.71073
Crystal system	triclinic
Space group	$P\bar{1}$
a, *b*, *c* [Å]	12.849(4), 13.044(6), 16.246(7)
α, β, γ [°]	86.04(4), 83.76(3), 69.20(3)
V [Å^3]	2529.0(2)
Z	2
D [g·cm^{-3}]	1.339
μ [mm^{-1}]	0.930
F(000)	1040
Crystal size [mm]	0.5 × 0.25 × 0.25
Measured reflections	10264
Independent reflections	9805
Data/restraints/parameters	9805/0/570
$R[F^2 > 2\sigma(F^2)]$; $wR(F^2)$	0.0641; 0.1560
S	0.624
R_{int}	0.099
$\Delta\sigma_{max}$; $\Delta\sigma_{min}$ (e Å^3)	0.557; –0.897

CCDC785397 (for 1[BF_4]·CH_2Cl_2) contains the supplementary crystallographic data for this paper. These data can be obtained free of charge from The Cambridge Crystallographic Data Centre via www.ccdc.cam.ac.uk/data_request/cif.

Supporting Information (see footnote on the first page of this article): CV of **1**$^+$, IR spectroelectrochemistry of **L** and **1**$^+$ as well as UV/Vis/NIR spectroelectrochemistry of **L**.

Acknowledgments

B. S. is indebted to the Baden-Württemberg Stiftung and Fonds der Chemischen Industrie for financial support of this project. J. F. gives thanks for support from the Grant Agency of the Czech Republic (grant numbers 203/09/0705, 203/08/1157).

[1] D. M. Dooley, M. A. McGruil, D. E. Brown, P. N. Turowski, W. S. McIntire, P. F. Knowles, *Nature* **1991**, *349*, 262.
[2] J. E. Dove, J. P. Klinmann, *Adv. Prot. Chem.* **2001**, *58*, 141.
[3] D. M. Dooley, *J. Biol. Inorg. Chem.* **1999**, *4*, 1.
[4] Y. Matobo, T. Kumagai, A. Yamamoto, H. Yoshitsu, M. Sugiyama, *J. Biol. Chem.* **2006**, *281*, 8981.
[5] H. Decker, T. Schweikardt, F. Tuczek, *Angew. Chem. Int. Ed.* **2006**, *45*, 4546.
[6] C. G. Pierpont, *Coord. Chem. Rev.* **2001**, *216–217*, 95.
[7] D. N. Hendrikson, C. G. Pierpont, *Top. Curr. Chem.* **2004**, *234*, 63.
[8] W. Kaim, *Dalton Trans.* **2003**, 761.
[9] C. G. Pierpont, C. W. Lange, *Prog. Inorg. Chem.* **1994**, *41*, 331.

[10] A. L. Balch, F. Röhrscheid, R. H. Holm, *J. Am. Chem. Soc.* **1965**, *87*, 2301.
[11] P. Chaudhuri, C. N. Verani, E. Bill, E. Boethe, T. Weyhermüller, K. Wieghardt, *J. Am. Chem. Soc.* **2001**, *123*, 2213.
[12] M. M. Khusniyarov, E. Bill, T. Weyhermüller, E. Boethe, K. Harms, J. Sundermeyer, K. Wieghardt, *Chem. Eur. J.* **2008**, *14*, 7608.
[13] C. A. Mitsopoulou, *Coord. Chem. Rev.* **2010**, *254*, 1448.
[14] P. Deplano, L. Pilia, D. Espa, M. L. Mercuri, A. Serpe, *Coord. Chem. Rev.* **2010**, *254*, 1434.
[15] A. I. Poddel'syk, V. I. Cherkasov, G. A. Abakumov, *Coord. Chem. Rev.* **2009**, *253*, 291.
[16] M. R. Haneline, A. F. Heyduk, *J. Am. Chem. Soc.* **2006**, *128*, 8410.
[17] M. R. Ringenberg, S. L. Kokatam, Z. M. Heiden, T. B. Rauchfuss, *J. Am. Chem. Soc.* **2008**, *130*, 788.
[18] T. Storr, P. Verma, R. C. Pratt, E. C. Wasinger, Y. Shimazaki, T. D. P. Stack, *J. Am. Chem. Soc.* **2008**, *130*, 15448.
[19] S. Bhattacharya, P. Gupta, F. Basuli, C. G. Pierpont, *Inorg. Chem.* **2002**, *41*, 5810.
[20] A. B. P. Lever, *Coord. Chem. Rev.* **2010**, *254*, 1397.
[21] S. Patra, B. Sarkar, S. M. Mobin, W. Kaim, G. K. Lahiri, *Inorg. Chem.* **2003**, *42*, 6469.
[22] H. Masui, A. L. Freda, M. C. Zerner, A. B. P. Lever, *Inorg. Chem.* **2000**, *39*, 141.
[23] S. Kar, B. Sarkar, S. Ghumaan, D. Janardanan, J. v. Slageren, J. Fiedler, V. G. Puranik, R. B. Sunoj, W. Kaim, G. K. Lahiri, *Chem. Eur. J.* **2005**, *11*, 4901.
[24] D. Kumbhakar, B. Sarkar, S. Maji, S. M. Mobin, J. Fiedler, F. A. Urbanos, R.-J. Aparicio, W. Kaim, G. K. Lahiri, *J. Am. Chem. Soc.* **2008**, *130*, 17575.
[25] H. S. Das, A. K. Das, R. Pattacini, R. Huebner, B. Sarkar, P. Braunstein, *Chem. Commun.* **2009**, 4387.
[26] H. S. Das, F. Weisser, D. Schweinfurth, C.-Y. Su, L. Bogani, J. Fiedler, B. Sarkar, *Chem. Eur. J.* **2010**, *16*, 2977.
[27] J. Maurer, M. Linseis, B. Sarkar, B. Schwederski, M. Niemeyer, W. Kaim, S. Zalis, C. Anson, M. Zabel, R. F. Winter, *J. Am. Chem. Soc.* **2008**, *130*, 259.
[28] M. Fabre, J. Bonvoisin, *J. Am. Chem. Soc.* **2007**, *129*, 1434.
[29] S. D. J. McKinnon, B. O. Patrick, A. B. P. Lever, R. G. Hicks, *Chem. Commun.* **2010**, *46*, 773.
[30] B. Podeszwa, H. Niedbala, J. Polanski, R. Musiol, D. Tabak, J. Finster, K. Serafin, M. Milczarek, J. Wietrzyk, S. Boryczka, W. Mol, J. Jampilek, J. Dohnal, D. S. Kalinowski, D. R. Richardson, *Bioorg. Med. Chem. Lett.* **2007**, *17*, 6138.
[31] M. Hassani, W. Cai, D. C. Holley, J. P. Lineswala, B. R. Maharjan, G. R. Ebrahimian, H. Seradj, M. G. Stocksdale, F. Mohammadi, C. C. Marvin, J. M. Gerdes, H. D. Beall, M. Behforouz, *J. Med. Chem.* **2005**, *48*, 7733.
[32] M. Behforouz, J. Haddad, W. Cai, M. B. Arnold, F. Mohammadi, A. C. Sousa, M. A. Horn, *J. Org. Chem.* **1996**, *61*, 6552.
[33] P. Braunstein, D. Bubrin, B. Sarkar, *Inorg. Chem.* **2009**, *48*, 2534.
[34] A. Paretzki, R. Pattacini, R. Huebner, P. Braunstein, B. Sarkar, *Chem. Commun.* **2010**, *46*, 1497.
[35] S. Roy, B. Sarkar, D. Bubrin, M. Niemeyer, S. Zalis, G. K. Lahiri, W. Kaim, *J. Am. Chem. Soc.* **2008**, *130*, 15230.
[36] C. Femoni, M. C. Iapalucci, G. Longoni, P. H. Svensson, P. Zanello, F. F. d. Biani, *Chem. Eur. J.* **2004**, *10*, 2318.
[37] T. Sixt, J. Fiedler, W. Kaim, *Inorg. Chem. Commun.* **2000**, *3*, 80.
[38] Y. Kasahara, Y. Hoshino, K. Shimizu, G. P. Sato, *Chem. Lett.* **1990**, 381.
[39] J. Diez, M. P. Gamasa, J. Gimeno, A. Aguirre, S. Garcia-Granda, *Organometallics* **1999**, *18*, 662.
[40] M. Behforouz, Z. Gu, W. Cai, M. A. Horn, M. Ahmadian, *J. Org. Chem.* **1993**, *58*, 7089.
[41] G. M. Sheldrick, *SHELXS-97, Program for Solution of Crystal Structures*, University of Göttingen, Germany, **1997**.

Received: January 4, 2011
Published Online: April 5, 2011

